PHYSICAL REVIEW A VOLUME 24, NUMBER 1 JULY 1981

Doubly differential cross sections of secondary electrons ejected from gases by electron impact: 25–250 eV on H_2

T. W. Shyn and W. E. Sharp
Space Physics Research Laboratory, University of Michigan, Ann Arbor, Michigan 48109

Y.-K. Kim
Argonne National Laboratory, Argonne, Illinois 60439

(Received 15 January 1981)

Doubly differential cross sections of secondary electrons ejected from H_2 by electron impact have been measured by a crossed-beam method. The incident energies used were 25, 40, 60, 100, 150, and 250 eV. The energy and angular range of secondary electrons measured were from one half of the difference between incident energy and ionization potential to 1.0 eV and from 12° to 156°, respectively. The present results do not agree with those of DuBois and Rudd for slow secondary electrons (< 20 eV) ejected by 100-eV primary electrons. The present data lead to total ionization cross sections within 10% of other measurements.

I. INTRODUCTION

Total ionization cross sections of H_2 by electron impact have been measured by several investigators (Tate and Smith,[1] Harrison,[2] Rapp and Englander-Golden,[3] and Schram *et al.*[4]) from threshold energy to 30 keV. However, the doubly differential cross sections (DDCS) of secondary electrons ejected from H_2 by electron impact have been measured only at two incident energies; 100 eV (DuBois and Rudd[5]) and 500 eV (Opal *et al.*[6]). In these DDCS measurements, the lowest secondary-electron energy attained was 4 eV.

The hydrogen molecule is the simplest molecule to study theoretically as well as experimentally. It is also an important molecule in the applied fields of study such as planetary atmospheres (Jupiter and Saturn) and chemical physics.

This paper presents the results of extensive measurements of secondary electrons ejected from H_2 by electron impact at six incident energies between 25 and 250 eV. The angular and energy range of secondary electrons measured were from 12° to 156° and from half of the difference between the incident energy and ionization potential to 1.0 eV, respectively. A crossed-beam method was used. The present results do not distinguish different modes of ionization, e.g., single ionization, double ionization, and dissociative ionization events.

II. APPARATUS AND PROCEDURE

The apparatus used for the present measurements is the same as that used previously[7,8] for the measurements of DDCS of secondary electrons ejected from He and CO_2, and detailed descriptions can be found in Ref. 7. A brief description of the apparatus is as follows: A rotatable electron beam in a horizontal plane interacts at 90° with a vertically collimated neutral beam. Secondary electrons ejected from the neutral beam were detected in a detector system fixed at the vacuum wall after energy analysis. When the neutral beam of H_2 was on, the background pressure rose to 4×10^{-5} torr and the density of the beam in the interaction region was estimated to be three times larger than the background density.

Compensation of the stray magnetic fields in the plane of the measurements was accomplished with three orthogonal Helmholtz coils down to less than 10 mG in all directions. The absolute energy scale was determined frequently to within 0.05 eV using the He resonance at 19.3 eV.

The procedure used for the present measurements was the same as the previous measurements of He and CO_2. The collimated H_2 beam was turned on and at a given incident energy the signal was integrated for 10 sec at each secondary-electron energy and each scattering angle from 12° to 156° in 12° increments. The measurements were repeated with the neutral beam off to obtain the background counts. The difference between the two signals yields the DDCS of secondary electrons ejected from the H_2 beam.

The correction of the final data for the pathlength effect due to the background density has been made (details of the correction can be found elsewhere[9]). The contribution of the background density to the total signal has been measured at 90° to 38 ± 2%.

III. EXPERIMENTAL RESULTS

The DDCS of secondary electrons have been measured at the incident energies of 25, 40, 60, 100, 150, and 250 eV. The results have been calibrated among themselves by normalizing the scattered signal against the incident current and target gas density for each incident and secondary electron energy and scattering angle. The nor-

malized results have been placed on an absolute scale using the elastic scattering cross sections of H_2 at 40 eV measured by Shyn and Sharp.[10] The H_2 elastic cross section has been normalized to the experimentally determined cross section[9] for He, which has been normalized to that calculated by Nesbet[11] at 10 eV.

The statistical uncertainty of the data points was less than 4% except for low secondary-electron energies (<3 eV) at small angles (<24°). The upper limit of the uncertainty in the data points at 12° was estimated to be 15%. There is 8% uncertainty in the intersecondary electron energy calibration and 7% in the interincident energy calibration. The normalization process of the present results to the elastic scattering cross sections of H_2 at 40 eV including the uncertainty in He elastic cross sections contains 10% uncertainty. The pathlength correction has 2% uncertainty except at 12° and the transmission has 5% uncertainty. Thus, the resultant uncertainty of the present results is ±16%.

Absolute cross sections for the six incident energies studied are shown in Tables I–VI. As noted earlier, the present results contain the contributions from dissociative ionization, single ionization, and double ionization.

Figure 1 shows a three-dimensional perspective diagram of secondary electrons ejected from H_2 by 40-eV electron impact. The angular distribution tends to be symmetric about 90° with a strong forward and backward scattered component at low secondary energies (<5 eV). At higher energies, the backward scattered component diminishes much faster than the forward scattered component.

Figure 2 shows a three-dimensional perspective diagram of secondary electrons ejected from H_2 by 250-eV electron impact. The angular distributions are slightly peaked toward forward scattering for secondary energies below 5 eV. Above 5 eV, the forward peak remains stronger as the secondary energy increases and a secondary maximum begins to emerge. This peak in DDCS near 60° is due to the conservation of energy and momentum of the colliding system. It is commonly referred to as the binary collision peak. The peak moves toward large angles, reaching a maximum angle near 10 eV, then returns to smaller angles as the secondary-electron energy increases as expected. This peak is clearly observable above 40-eV incident energy.

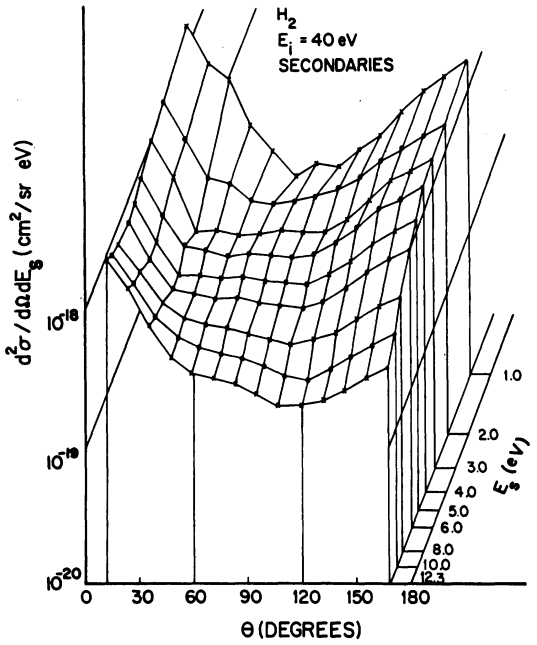

FIG. 1. Three-dimensional plot of secondary electrons ejected from H_2 by 40-eV incident electrons as functions of ejection angle θ and secondary energy E_s.

Figure 3 compares the angular distribution at the secondary-electron energy of 4 and 35 eV for 100-eV incident electrons, along with the results of DuBois and Rudd.[5] The agreement between the present results and the measurements by DuBois and Rudd for low secondary energy (4 eV) is poor, particularly in shape. Agreement is much better for the secondary energy of 35 eV.

At present there is no reliable theory for the angular distribution of the secondary electrons from molecules valid for the intermediate inci-

TABLE I. DDCS ($d^2\sigma/d\Omega\,dE$) of secondary electrons ejected from H_2 by 25-eV electron impact (in units of 10^{-20} cm^2/sr eV). (The numbers in parentheses represent extrapolated data points.)

E_s(eV) \ θ°	12	24	36	48	60	72	84	96	108	120	132	144	156	168	$\Delta\sigma/\Delta E$ (10^{-18} cm^2/eV)
1.0	141.6	71.9	59.6	33.4	22.8	21.0	24.5	22.8	24.6	35.1	49.1	59.6	73.6	(96.4)	9.69
2.0	90.4	45.1	40.9	28.3	29.6	27.6	29.6	31.9	42.8	47.0	56.5	74.7	94.0	(117.3)	9.94
3.0	74.7	51.4	28.2	26.8	22.6	25.1	26.4	27.1	29.3	36.3	51.1	70.1	86.7	(112.3)	8.80
4.0	96.8	63.0	35.0	29.4	22.0	24.3	23.6	25.2	27.0	30.7	43.7	57.2	69.3	(83.8)	8.32
4.8	105.1	62.6	32.2	31.4	21.7	22.0	22.8	23.5	25.2	29.3	38.4	55.4	75.8	(100.3)	8.50

TABLE II. DDCS ($d^2\sigma/d\Omega\,dE$) of secondary electrons ejected from H_2 by 40-eV electron impact (in units of 10^{-20} cm^2/sr eV). (The numbers in parentheses represent extrapolated data points.)

E_s(eV) \ $\theta°$	12	24	36	48	60	72	84	96	108	120	132	144	156	168	$\Delta\sigma/\Delta E$ (10^{-18} cm^2/eV)
1.0	439.3	241.8	176.6	81.4	53.4	46.5	55.9	53.4	65.0	79.0	100.0	139.5	186.0	(237.1)	12.4
2.0	300.0	153.7	83.3	73.8	55.1	52.9	55.1	60.1	65.3	79.9	103.7	127.7	159.6	(191.1)	10.6
3.0	252.6	135.1	55.8	57.2	51.4	52.8	55.7	54.3	54.3	65.4	91.0	124.8	148.3	(182.0)	9.62
4.0	193.0	99.5	62.0	58.0	53.0	54.8	53.7	50.2	53.0	64.8	82.4	112.2	131.0	(158.7)	9.02
5.0	172.5	89.8	51.7	51.7	50.2	50.2	48.6	45.7	45.7	51.7	65.4	85.4	105.4	(127.9)	7.72
6.0	157.7	83.2	51.6	48.2	44.5	45.7	42.9	40.0	38.3	42.5	52.9	68.7	84.6	(102.1)	6.69
8.0	167.2	100.9	62.8	48.8	43.1	40.5	37.1	33.3	30.6	32.6	36.9	46.2	57.1	(67.8)	5.87
10.0	191.5	116.9	66.3	47.3	39.4	35.9	32.9	28.4	24.9	23.8	27.2	33.7	40.1	(49.4)	5.26
12.3	227.6	140.8	76.2	44.3	34.1	31.3	28.2	23.6	19.9	19.3	20.5	25.0	30.2	(36.1)	5.02

TABLE III. DDCS ($d^2\sigma/d\Omega\,dE$) of secondary electrons ejected from H_2 by 60-eV electron impact (in units of 10^{-20} cm^2/sr eV). (The numbers in parentheses represent extrapolated data points.)

E_s(eV) \ $\theta°$	12	24	36	48	60	72	84	96	108	120	132	144	156	168	$\Delta\sigma/\Delta E$ (10^{-18} cm^2/eV)
1.0	452.6	253.6	130.0	67.1	65.0	58.6	56.6	62.9	60.8	67.1	79.4	108.9	148.8	(192.8)	12.3
2.0	237.0	105.1	87.6	71.1	61.7	63.3	64.3	64.3	72.2	80.7	100.7	132.0	175.3	(223.2)	11.2
3.0	167.4	83.4	47.5	63.9	63.9	66.6	65.5	66.6	70.0	79.5	97.3	127.6	160.7	(198.8)	10.3
4.0	119.3	47.0	35.6	56.7	59.6	58.9	57.1	53.9	58.2	65.4	81.6	101.2	111.6	(129.1)	8.70
5.0	103.9	52.7	34.7	57.8	61.0	59.2	56.9	53.7	52.7	56.9	66.9	84.5	99.6	(116.4)	7.88
6.0	82.0	45.8	33.8	51.6	55.8	54.9	49.8	43.9	40.3	43.5	50.7	63.9	75.4	(89.7)	6.42
8.0	79.0	43.0	31.1	43.4	46.2	44.8	39.6	33.0	29.1	29.3	33.9	40.6	47.9	(57.2)	4.93
10.0	75.5	52.3	40.7	39.6	41.1	37.9	32.8	26.2	21.9	22.6	25.3	29.3	33.2	(37.2)	4.21
12.0	64.3	46.2	36.3	34.1	33.3	30.7	24.7	19.1	16.1	15.5	16.7	19.3	21.7	(24.4)	3.26
15.0	59.2	41.9	31.1	26.1	24.2	21.4	16.7	12.7	10.3	10.3	11.3	12.5	14.7	(17.3)	2.40
20.0	76.0	53.4	34.8	24.7	20.5	16.8	12.6	8.81	6.88	5.94	6.24	6.78	7.82	(8.86)	2.14
22.3	89.2	59.5	36.2	23.9	18.7	14.6	10.8	7.87	5.90	4.92	4.97	5.50	6.39	(7.33)	2.00

TABLE IV. DDCS ($d^2\sigma/d\Omega\, dE$) of secondary electrons ejected from H_2 by 100-eV electron impact (in units of 10^{-20} cm^2/sr eV). (The numbers in parentheses represent extrapolated data points.)

E_s(eV) \ θ°	12	24	36	48	60	72	84	96	108	120	132	144	156	168	$\Delta\sigma/\Delta E$ (10^{-18} cm^2/eV)
1.0	394.6	189.6	133.3	82.0	42.8	42.8	33.8	39.3	46.1	47.8	53.0	56.4	72.6	(85.4)	8.79
2.0	218.9	84.1	64.3	58.0	52.5	48.4	47.8	47.8	51.9	56.0	68.4	80.3	101.7	(130.7)	8.26
3.0	135.4	58.4	56.0	47.4	50.7	52.4	52.0	52.0	54.7	59.0	68.1	81.0	100.4	(113.6)	7.39
4.0	105.2	45.9	36.0	41.9	45.2	51.5	50.0	46.4	48.8	49.1	58.1	70.4	75.8	(81.7)	6.55
5.0	81.8	41.8	36.3	44.0	51.0	49.9	46.3	43.5	39.7	42.5	47.7	56.4	60.9	(65.8)	5.92
6.0	72.5	35.1	28.2	44.6	49.7	48.1	44.1	39.2	34.9	35.3	40.3	45.4	49.5	(53.7)	5.31
8.0	61.1	36.7	33.5	38.0	44.3	41.7	38.5	29.8	26.0	25.7	28.0	32.6	35.9	(39.5)	4.38
10.0	49.3	36.7	29.0	36.1	38.0	36.5	30.0	23.7	19.4	17.8	18.7	21.6	22.8	(24.2)	3.49
12.0	45.6	31.0	27.4	32.5	37.1	34.1	27.9	20.9	16.5	15.2	16.1	17.9	20.0	(22.0)	2.47
15.0	34.2	24.7	19.2	22.2	22.5	20.6	15.6	10.9	8.48	7.93	8.30	9.58	11.1	(12.8)	1.90
20.0	19.3	14.6	12.0	14.8	16.7	14.0	9.49	5.93	4.21	3.90	3.79	4.30	4.81	(5.32)	1.13
25.0	17.1	12.8	11.5	12.2	11.7	8.57	4.92	3.33	2.34	1.86	1.86	2.02	2.30	(2.54)	0.79
30.0	15.1	11.2	10.4	10.9	9.63	6.48	3.79	2.23	1.52	1.35	1.24	1.35	1.49	(1.66)	0.64
35.0	15.7	11.8	10.7	10.0	7.66	4.72	2.58	1.57	1.07	0.92	0.92	0.98	1.04	(1.07)	0.54
40.0	20.5	16.1	13.6	11.0	7.06	4.12	2.25	1.36	0.87	0.72	0.63	0.72	0.84	(0.98)	0.53
42.3	21.5	19.7	15.8	11.4	7.12	3.86	2.13	1.30	0.86	0.75	0.66	0.66	0.81	(0.98)	0.53

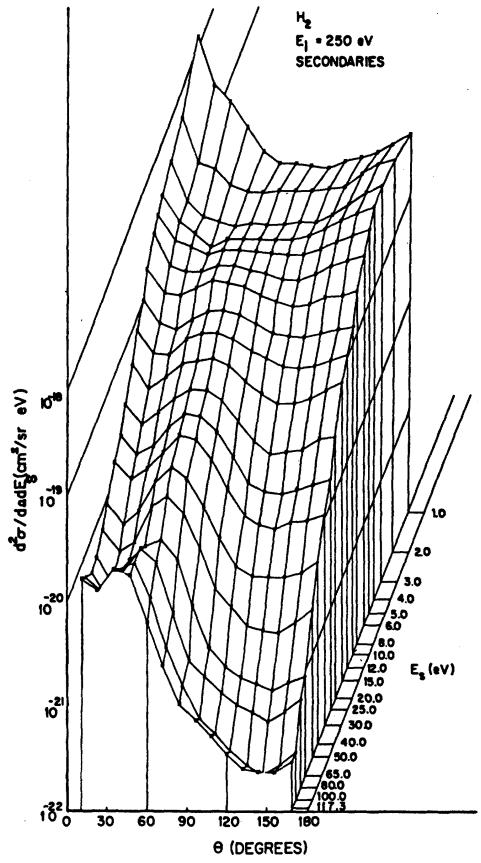

FIG. 2. Same as Fig. 1 by 250-eV incident electrons.

dent energies used in our experiment. For the time being, the reliability and consistency of our results can be examined only indirectly by studying the singly differential cross section

$$\frac{d\sigma}{dE_s}=\int\left(\frac{d^2\sigma}{d\Omega\, dE_s}\right)d\Omega\,, \tag{1}$$

and the total ionization cross section

$$\sigma_i=\int_0^{(E_s)_{\max}}\left(\frac{d\sigma}{dE_s}\right)dE_s\,, \tag{2}$$

derived from the angular distributions. The maximum energy of the secondary electron is defined by

$$(E_s)_{\max}=\tfrac{1}{2}(E_i-B)\,, \tag{3}$$

where E_i is the incident (=primary) electron energy, and B is the first ionization potential of the molecule.

IV. INTEGRATED AND TOTAL IONIZATION CROSS SECTIONS

To obtain singly differential cross sections, angular distributions must be extrapolated to for-

TABLE V. DDCS ($d^2\sigma/d\Omega\, dE$) of secondary electrons ejected from H_2 by 150-eV electron impact (in units of 10^{-20} cm^2/sr eV). (The numbers in parentheses represent extrapolated data points.)

E_s(eV) \ $\theta°$	12	24	36	48	60	72	84	96	108	120	132	144	156	168	$\Delta\sigma/\Delta E$ (10^{-18} cm^2/eV)
1.0	532.4	146.1	103.6	69.0	42.4	40.8	39.3	40.9	45.5	44.0	50.3	58.1	62.9	(69.0)	8.11
2.0	232.0	92.1	67.4	53.9	52.5	43.5	43.3	47.1	51.0	53.5	60.6	69.8	83.9	(100.7)	7.70
3.0	142.0	59.0	37.7	33.8	45.2	46.7	45.5	45.9	47.3	48.5	57.2	64.4	83.6	(109.1)	6.64
4.0	97.8	52.8	36.2	39.5	45.9	47.6	44.1	43.9	44.2	46.4	51.2	60.2	66.5	(73.6)	6.05
5.0	70.5	39.9	34.4	36.1	45.5	47.4	45.7	41.1	38.6	39.7	44.2	51.3	55.3	(59.4)	5.51
6.0	65.3	31.4	29.4	39.6	43.3	42.8	39.6	35.2	31.9	31.8	35.1	40.2	45.5	(51.1)	4.78
8.0	41.5	27.1	21.6	33.6	36.1	36.9	32.3	26.1	22.9	21.1	22.9	26.7	29.6	(32.7)	3.60
10.0	34.2	23.1	21.2	24.6	30.1	29.3	24.7	19.9	15.3	14.9	15.0	17.3	18.7	(20.1)	2.78
12.0	25.1	14.9	15.9	19.8	23.9	23.6	20.0	14.8	11.6	10.3	11.2	12.1	13.5	(15.1)	2.07
15.0	17.1	12.4	11.5	15.7	17.5	17.7	13.4	9.76	7.26	6.72	7.00	7.54	8.45	(9.44)	1.45
20.0	12.8	8.73	9.32	11.3	13.5	12.1	8.63	5.33	3.68	3.03	3.03	3.20	3.44	(3.72)	0.93
25.0	7.32	5.42	6.31	9.10	10.8	9.10	5.59	3.27	2.10	1.56	1.62	1.86	2.03	(2.16)	0.63
30.0	5.22	2.93	4.46	7.54	8.58	6.63	3.69	2.15	1.27	1.04	1.02	1.11	1.32	(1.53)	0.45
35.0	4.08	3.24	3.20	6.40	6.55	4.82	2.59	1.30	0.84	0.65	0.63	0.69	0.76	(0.86)	0.34
40.0	3.70	2.40	3.85	5.92	5.94	3.65	1.78	0.95	0.67	0.52	0.52	0.48	0.57	(0.67)	0.29
50.0	4.02	3.37	4.24	5.47	4.75	2.19	1.02	0.54	0.39	0.29	0.28	0.26	0.29	(0.33)	0.23
60.0	5.22	4.53	5.48	5.26	3.33	1.42	0.60	0.30	0.25	0.17	0.18	0.18	0.24	(0.32)	0.21
67.3	6.53	6.13	6.33	5.38	2.39	1.02	0.45	0.25	0.17	0.17	0.19	0.17	0.20	(0.25)	0.21

TABLE VI. DDCS ($d^2\sigma/d\Omega\,dE$) of secondary electrons ejected from H_2 by 250-eV electron impact (in units of 10^{-20} cm^2/sr eV). (The numbers in parentheses represent extrapolated data points.)

E_s(eV) \ $\theta°$	12	24	36	48	60	72	84	96	108	120	132	144	156	168	$\Delta\sigma/\Delta E$ (10^{-18} cm^2/eV)
1.0	429.4	143.5	103.1	60.4	35.3	26.4	26.4	25.1	24.0	27.6	30.1	34.1	41.6	(50.9)	6.23
2.0	175.3	65.5	59.4	40.9	35.1	34.8	36.1	36.4	36.1	37.4	39.6	52.8	65.0	(71.9)	5.80
3.0	110.7	46.0	32.7	30.0	27.0	29.0	27.5	27.5	30.0	29.8	35.0	45.0	54.5	(66.5)	4.94
4.0	75.0	42.3	32.2	25.2	29.3	29.3	28.7	28.4	28.9	31.5	36.5	44.6	51.7	(59.8)	4.33
5.0	64.8	38.7	32.7	28.5	30.9	30.7	30.4	28.7	29.3	27.8	31.8	36.9	42.4	(48.8)	4.05
6.0	54.7	27.7	24.5	24.8	27.9	28.2	25.6	23.7	20.6	20.5	23.4	28.0	30.9	(34.1)	3.62
8.0	37.8	22.4	21.7	25.2	29.8	28.7	26.1	21.0	18.6	16.8	17.5	20.2	21.8	(23.6)	2.88
10.0	27.5	16.4	14.7	18.9	21.4	22.2	20.1	16.1	13.4	12.2	12.1	13.4	14.3	(15.3)	2.10
12.0	17.7	10.8	10.3	14.1	16.5	16.8	14.4	11.0	9.26	7.84	7.54	7.83	8.85	(10.1)	1.47
15.0	11.2	6.64	8.67	11.8	13.0	13.3	11.3	7.99	6.11	5.00	5.15	5.53	6.64	(7.99)	1.10
20.0	7.01	4.41	5.89	8.01	9.82	9.71	7.36	4.83	3.03	2.35	2.46	2.60	3.24	(3.46)	0.693
25.0	4.80	3.20	3.94	5.81	7.97	7.59	5.24	3.06	1.73	1.41	1.35	1.49	1.64	(1.81)	0.488
30.0	3.46	2.40	2.99	4.35	6.21	5.78	3.65	1.90	1.06	0.87	0.80	0.94	0.99	(1.10)	0.350
40.0	2.04	1.32	1.78	3.31	4.60	3.59	1.96	0.94	0.50	0.40	0.40	0.38	0.43	(0.54)	0.214
50.0	1.58	0.98	1.26	2.66	3.38	2.26	1.05	0.43	0.29	0.19	0.17	0.16	0.20	(0.27)	0.142
65.0	1.27	0.71	1.11	2.05	2.32	1.22	0.44	0.17	0.11	0.087	0.076	0.066	0.076	(0.090)	0.090
80.0	1.13	0.68	1.21	2.00	1.46	0.48	0.17	0.12	0.080	0.063	0.053	0.044	0.053	(0.072)	0.064
100.0	1.53	1.10	1.74	2.13	0.94	0.33	0.14	0.064	0.047	0.032	0.024	0.020	0.024	(0.032)	0.063
117.3	1.73	1.33	2.16	1.83	0.65	0.25	0.11	0.080	0.056	0.038	0.027	0.025	0.025	(0.031)	0.061

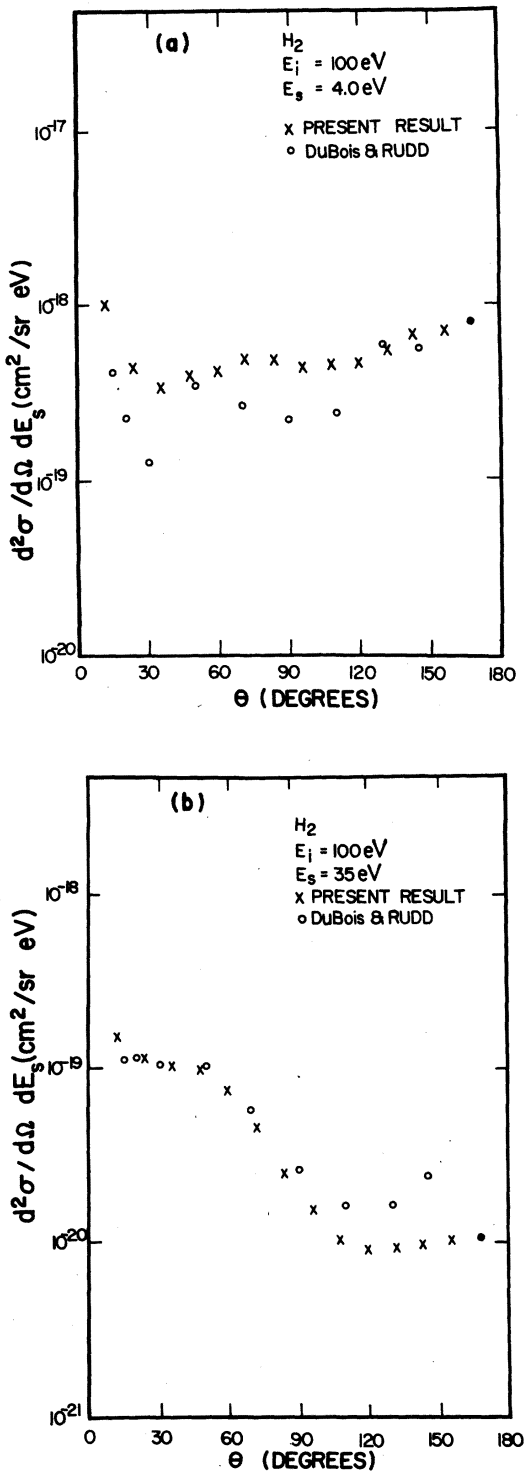

FIG. 3. Comparison of secondary-electron angular distributions. Circles represent electron-impact data by DuBois and Rudd (Ref. 5). All data are from the incident energy by 100 eV. Filled circles at $\theta = 168°$ are extrapolated data from our measurements. (a) Secondary-electron energy at 4 eV and (b) secondary-electron energy at 35 eV.

ward and backward angles not covered by the experiment. Extrapolated data at $\theta = 168°$ are presented in parentheses in Tables I–VI. Fortunately, the angular distributions at $\theta = 0°$ and 180° are not needed because $\sin\theta$ in $d\Omega = 2\pi \sin\theta\, d\theta$ vanishes there. Also, because of the $\sin\theta$ factor, $d\sigma/dE_s$ from different experiments will disagree only when their angular distributions disagree around $\theta \sim 90°$. Figure 3(a) is such an example. On the other hand, the example shown in Fig. 3(b) will lead to similar $d\sigma/dE_s$.

Figure 4 shows our $d\sigma/dE_s$ at $E_i = 100$ eV, along with those of DuBois and Rudd.[5] There is good agreement between the present results and those of DuBois and Rudd above 25-eV secondary energies. Below 25 eV, their values are smaller than the present results by as much as 50% because their angular distributions are smaller than those reported here.

To obtain σ_i from $d\sigma/dE_s$, the singly differential cross section must be extrapolated over the ranges of E_s not covered in an experiment. It is convenient to use the Platzman plot[12] for such extrapolations.

In the Platzman plot, the ordinate is the ratio of $d\sigma/dE_s$ to the Rutherford cross section and the abscissa is the inverse of the energy transfer, $E_t = E_s + B$. For simplicity, we use only the lowest ionization potential ($B = 15.43$ eV) in the Platzman plot. This is equivalent to a simplified assump-

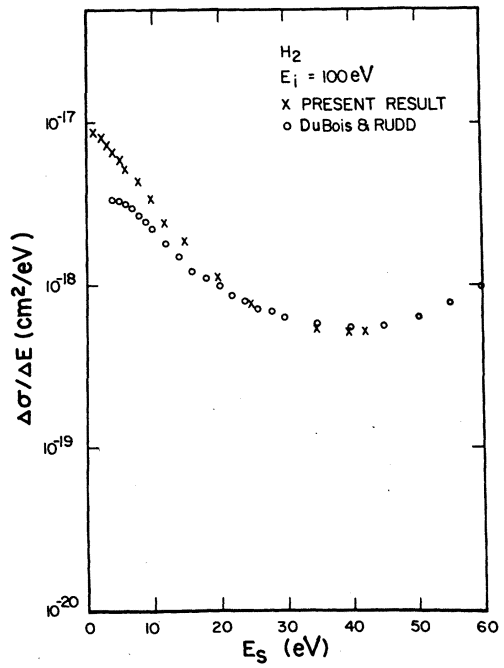

FIG. 4. Comparison of energy distributions of secondary electrons ejected by 100 incident electrons. Circles are the data from Ref. 5.

tion that all H_2^+ ions are produced in the ground state. The Platzman plot offers the following advantages. (a) The plot clearly illustrates the qualitative shift in the shape of $d\sigma/dE_s$ as the incident energy E_i is increased. At high E_i(> 500 eV), the Born approximation predicts[12] that the overall shape of $d\sigma/dE_s$ should resemble the shape of corresponding photoionization cross sections. (b) The plot allows easy extrapolation of $d\sigma/dE_s$ to the values of E_s not covered by the experiment. (c) The area under the Platzman plot bounded between $E_s = 0$ and $(E_s)_{max}$ (including the extrapolations mentioned above) is directly proportional to σ_i. The proportionality constant is known, and σ_i can be put on an absolute scale, either for comparison with other values of σ_i or, if reliable σ_i is available, for normalization of the secondary-electron distributions.

The Platzman plots of our results are presented in Fig. 5. The ordinate of Fig. 5, $Y(E_s)$, is defined by

$$Y(E_s) = \frac{d\sigma}{dE_s} \Big/ \left(\frac{d\sigma}{dE_s}\right)_{\text{Ruth}}, \tag{4}$$

where the Rutherford cross section is given by

$$\left(\frac{d\sigma}{dE_s}\right)_{\text{Ruth}} = \frac{4\pi a_0^2}{E_i}\left(\frac{R}{E_t}\right)^2. \tag{5}$$

In Eq. (5), $a_0 = 0.529$ Å is the Bohr radius and R = 13.6 eV is the Rydberg energy. Equation (5) is an adaptation of the Rutherford cross section for a free electron,[13] in which E_s is used instead of the energy transfer E_t. For fast secondary electrons, $E_s \gg B$ and Eq. (5) will approach the free-electron Rutherford cross section. Qualitatively, $Y(E_s)$ corresponds to the effective number of electrons participating in ionizing collisions. Large values of $Y(E_s)$ for slow secondary electrons as E_i is increased, stem from the growing contribution of the dipole-allowed interaction.

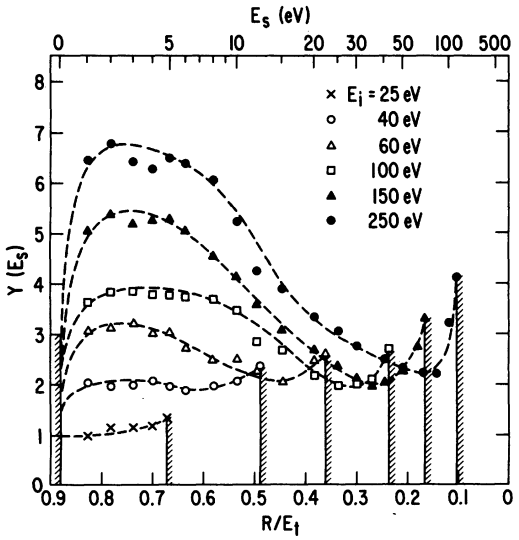

FIG. 5. The Platzman plots of the present results at various incident energies, E_i. The abscissa is the inverse of the energy transfer E_t in rydbergs, and the ordinate is the ratio of the energy distribution to the Rutherford cross section. Secondary-electron-energy scale is on the top. Area under each Platzman plot bounded by the hatched lines gives the total ionization cross section σ_i as explained in the text. Broken curves were used to obtain σ_i from our data.

According to the Born approximation, $d\sigma/dE_s$ can be qualitatively divided into two parts; the dipole-allowed part (known as the glancing collision) that should resemble the photoionization cross section *in shape*, and the nondipole part (known as the knock-on collision) that should resemble *in shape* the Rutherford (or Mott to account for the electron-exchange effect) cross section.

In Fig. 6 we present our $d\sigma/dE_s$ at $E_i = 250$ eV, electron-impact data at $E_i = 500$ eV by Opal, Beaty, and Peterson,[6] the Mott cross section[12] for H_2, and photoionization cross section by Samson and Haddad,[14] and those by Backx, Wight, and van der Wiel.[15] The data by Backx *et al.* were obtained by forward scattering of fast electrons to simulate photoionization.

Comparison of Figs. 5 and 6(a) with Fig. 6(b) clearly indicates the increasing contribution from the dipole interaction at higher E_i. The Platzman plots for $E_i < 50$ eV in Fig. 5 also show that $d\sigma/dE_s$ is affected very little by the dipole interaction.

To obtain σ_i, one integrates the area under the Platzman plot bounded between $E_s = 0$ and $(E_s)_{max}$:

$$\sigma_i = \int_0^{(E_s)_{max}} \frac{d\sigma}{dE_s}\, dE_s$$

$$= \frac{4\pi a_0^2}{E_i/R} \int_{x_0}^{x_{max}} Y(x)\, dx, \tag{6}$$

where $x = R/E_t$, $x_{max} = R/B$, and $x_0 = 2R/(E_i + B)$.

Examination of Fig. 6(a) clearly shows the importance of the data for $E_s < 10$ eV in order to determine σ_i accurately. For instance, the experimental data by Opal *et al.*[6] should be extrapolated upward to $E_s \sim 1.5$ eV and then reduced to a small value at threshold, as indicated by the broken curve. This leads to $\sigma_i \cong 0.59$ Å^2 contrary to their statement[6] that their data result in $\sigma_i = 0.40$ Å^2. The normalization of the data by Opal *et al.* for H_2 should be reduced by one-third to be consistent with the value $\sigma_i = 0.40$ Å^2 measured by Tate and Smith[1] and also by Rapp and Englander-Golden.[3]

The Mott cross section does not include the dipole interaction, and the difference between the

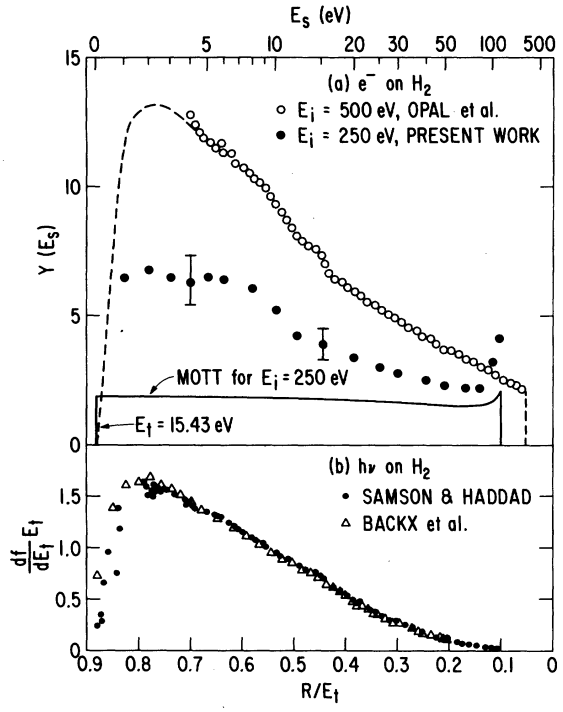

FIG. 6. Comparison of secondary-electron energy distributions and photoionization cross sections of H_2. (a) The Platzman plot of the electron-impact data by Opal, Beaty, and Peterson (Ref. 6) (circles) at 500-eV incident energy, and those by the present authors at 250-eV incident energy. Energy transfer of 15.43 eV is the first ionization potential of H_2, corresponding to the production of zero-kinetic-energy secondaries. The Mott cross section qualitatively represents that part of the ionization caused from knock-on (large momentum transfer) collisions. The broken curve was used in integrating the data by Opal *et al.* to obtain the total ionization cross section. (b) The continuum dipole oscillator strengths, df/dE_t, (E_t here is the photon energy) were derived from the photoionization measurement by Samson and Haddad (Ref. 14), and from the electron-impact data by Backx, Wight, and van der Wiel (Ref. 15). The ordinate of (b) represents *qualitatively* the contribution of dipole-allowed interaction; its shape should be compared to that of the difference between the electron-impact data and the Mott cross section in (a).

electron-impact data in Fig. 6(a) and the Mott cross section *qualitatively* represents the contribution from the dipole interaction, whose *shape* should resemble that of the plot in Fig. 6(b). In Figs. 5 and 6(a), the $Y(E_s)$ near the maximum secondary energies increase due to the exchange interaction, as is also the case for the Mott cross section. The data by Opal *et al.* in Fig. 6(a) do not turn upward because they did not measure high enough secondary energies.

With the help of the Platzman plot, we extrapolated and integrated our $d\sigma/dE_s$ to obtain σ_i, as indicated by the broken curves in Fig. 5. The results are presented in Table VII and also compared with direct measurements[1,3] of σ_i, as well as with those from other secondary-electron measurements[5,6] in Fig. 7. Our σ_i tends to be ~10% higher than those from Refs. 1 and 3. Renormalization of our data, however, should be done after reliable values of σ_i for H_2 have been adopted. Also, in principle, $d\sigma/dE_s$ at $E_s = 0$ should be a finite value—one can extrapolate from the discrete excitations if the cross sections for all Rydberg series are known.[16] The shape of the photoionization data in Fig. 6(b), however, suggests that the threshold values of $d\sigma/dE_s$ for H_2 will be small. Reliable data on $d\sigma/dE_s$ at $E_s = 0$ for various incident energies such as those measured by Grissom, Compton, and Garrett[17] for rare gases would be valuable in the accurate normalization of the secondary-electron data.

The discrepancy between our σ_i at $E_i = 100$ eV and that by DuBois and Rudd[5] is not surprising at all in view of their low cross sections for slow secondaries, as shown in Fig. 4. Although we did not present here the Platzman plot of the data by DuBois and Rudd, such a plot clearly indicates a growing tendency of low cross sections for $E_s < 25$ eV, resulting in the total ionization cross section of ~0.6 Å^2.

V. SUMMARY

Doubly differential cross sections of secondary electrons ejected from H_2 by electron impact have been measured utilizing a crossed-beam method in the incident-energy range from 25 to 250 eV. The energy and angular range of secondary electrons measured were from 1.0 eV to one half of the difference between incident energy and ionization potential and from 12° to 156°, respectively. The cross section shows a smooth systematic variation with both energy and angle. There is a general trend for strong forward scattering. It is found that other measurements[5] of doubly differential and singly differential cross sections differ with the present results in magnitudes and systematic

TABLE VII. Total ionization cross section obtained by integrating the singly differential cross section.

E_i (eV)	σ_i (Å^2)
25	0.43
40	0.93
60	1.10
100	0.97
150	0.86
250	0.68

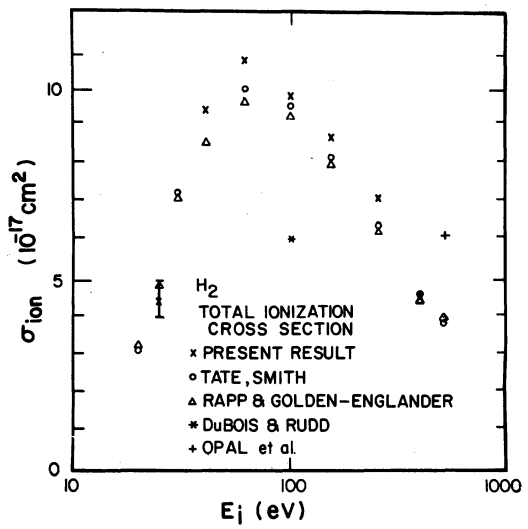

FIG. 7. Total ionization cross section of H_2 by electron impact along with other previous measurements.

behavior. In particular, the singly differential cross sections by DuBois and Rudd[5] at 100-eV incident energy are smaller than the present results by as much as 50% for slow (<25 eV) secondary electrons. The H_2 data by Opal, Beaty, and Peterson[6] should be reduced by one-third to be consistent with the total ionization cross section by Tate and Smith.[1] The total ionization cross sections obtained by integrating our data agree well (~10%) with those measured directly.[1,3]

ACKNOWLEDGMENTS

This work was supported by NSF under Grant No. ATM79-01618 and by the U.S. Department of Energy. The authors thank Winston Chang for his help in taking and analyzing the data, and Professor J. A. R. Samson for providing them with the photoionization cross section quoted in Fig. 6.

[1]J. T. Tate and P. T. Smith, Phys. Rev. 39, 270 (1932).
[2]H. Harrison, Ph.D. thesis, The Catholic University of America Press, Inc., Washington, D. C. (1956) (unpublished).
[3]D. Rapp and P. Englander-Golden, J. Chem. Phys. 43, 1464 (1965).
[4]B. L. Schram, F. J. de Heer, M. J. van der Wiel, and J. Kistemaker, Physica (Utrecht) 31, 94 (1964).
[5]R. D. DuBois and M. E. Rudd, Phys. Rev. A 17, 843 (1978).
[6]C. B. Opal, E. C. Beaty, and W. K. Peterson, At. Data 4, 209 (1972).
[7]T. W. Shyn and W. E. Sharp, Phys. Rev. A 19, 557 (1979).
[8]T. W. Shyn and W. E. Sharp, Phys. Rev. A 20, 2332 (1979).
[9]T. W. Shyn, Phys. Rev. A 22, 916 (1980).
[10]T. W. Shyn and W. E. Sharp (unpublished).
[11]R. K. Nesbet, Phys. Rev. A 20, 58 (1979).
[12]Y.-K. Kim, Radiat. Res. 61, 21 (1975); 64, 205 (1975).
[13]See, for instance, L. D. Landau and E. M. Lifshitz, *Quantum Mechanics* (Pergamon, New York, 1965), 2nd ed., footnote on p. 575.
[14]J. A. R. Samson and G. N. Haddad, personal communication. Their data are presented in J. A. R. Samson, Phys. Rep. 28C, 303 (1976), Fig. 9.
[15]C. Backx, G. R. Wight, and M. J. van der Wiel, J. Phys. B 9, 315 (1976).
[16]Y.-K. Kim and M. Inokuti, Phys. Rev. A 7, 1257 (1973).
[17]J. T. Grissom, R. N. Compton, and W. R. Garrett, Phys. Rev. A 6, 977 (1972).